



Inventory control assessment for small scale sCO₂ heat to power conversion systems

Matteo Marchionni^{*}, Muhammad Usman, Lei Chai, Savvas A. Tassou

Brunel University London, Institute of Energy Futures, Center for Sustainable Energy Use in Food Chains, Uxbridge, Middlesex, UB8 3PH, UK

ARTICLE INFO

Keywords:

Supercritical CO₂ power cycles
Waste heat recovery
Inventory control
Transient analysis
sCO₂ power cycle controls
Control design

ABSTRACT

The control of the main cycle parameters in supercritical CO₂ (sCO₂) systems during off-design and transient operation is crucial for advancing their technological readiness level. In smaller scale power units (<0.5–5 MW), costs and complexity constraints limit the number of auxiliary components in the power loop, making the design of the control system even more challenging.

Among the possible strategies, the regulation of system inventory, which consists in varying the CO₂ fluid mass in the power loop to achieve a given control target, represents a promising alternative. Such technique however poses several technical challenges that are still to be fully understood. To fill this gap, this work presents a comprehensive steady-state and transient analysis of inventory control systems, referring in particular to a 50 kW sCO₂ test facility being commissioned at Brunel University.

Stability implications (e.g. pressure gradients in the loop) and the effects of variable inventory tank size are discussed. Tank volumes 3 times higher than the one of the power loop (including the receiver) can lead to a higher controllability range ($\pm 30\%$ of the nominal turbine inlet temperature) and an extended availability of the control action (slower tank discharge). A PI controller is also designed to regulate the turbine inlet temperature around the target of 465 °C in response to waste heat variations.

1. Introduction

Recently, power cycles with carbon dioxide in the supercritical state (sCO₂) as the working fluid have received a strong interest by academia and industry [1]. Compared to state-of-the-art technologies such as steam and organic Rankine systems, sCO₂ systems have the following advantages: global conversion efficiency up to 10% higher (compared to other technologies) thanks to reduced compression work near the critical point (33.0 °C, 74 bar); better heat utilisation (exergy efficiency) due to absence of phase change during the heat recovery process; less cycle temperature limitations; higher power flexibility, along with smaller footprint, better water utilisation and higher thermal stability. Furthermore, CO₂ is an environmentally friendly working fluid, having unitary Global Warming Potential (GWP) and zero Ozone Depletion Potential (ODP).

The interest in sCO₂ technology goes beyond high temperature waste heat to power conversion [2] and covers the whole spectrum of power generation, from fossil fuel to nuclear and renewable applications. The high efficiency potential and extremely compact turbomachinery make it also an attractive alternative propulsion technology [3].

Research on sCO₂ power systems is currently focused on thermodynamic and techno-economic analyses to identify the optimal cycle layouts both using pure CO₂ or blends (mixtures of CO₂ and other fluids, often called dopants [4]) with additional focus areas related to investigations of performance at component level, i.e. turbomachinery and heat exchangers as well as at fundamental scale, i.e. flow topology in converging-diverging nozzles or heat transfer [1].

Studies on off-design and transient operating regimes of sCO₂ power systems are limited due to low availability of experimental datasets from the small pool of test facilities whose total world count is below 15 [2]. These reasons also reflect the scarce literature on the control of sCO₂ power cycles. In general, the sCO₂ control narratives are derived from closed loop Brayton cycle experiences with helium or argon [5]. However, the highly non-ideal nature of sCO₂ differentiates it from other Brayton cycles and introduces additional control considerations close to the critical point. For this reason, the majority of the works are focused on regulating the inlet conditions of the compressor and turbine to ensure the optimal and stable operation of the system.

Deviation in inlet density conditions can cause significant changes to flow conditions in the compressor leading to overall cycle performance and controllability issues. To operate the compressor in an optimal and

^{*} Corresponding author.s

E-mail address: matteo.marchionni2@brunel.ac.uk (M. Marchionni).

<https://doi.org/10.1016/j.energy.2022.126537>

Received 1 March 2022; Received in revised form 5 November 2022; Accepted 22 December 2022

Available online 26 December 2022

0360-5442/© 2023 The Authors. Published by Elsevier Ltd. This is an open access article under the CC BY license (<http://creativecommons.org/licenses/by/4.0/>).

Nomenclature**Symbols**

ξ	Pressure loss coefficient [-]
ρ	Density [kg/m^3]
σ	Surface tension [Pa]
ν	Dynamic viscosity [m^2/s]
dx	Displacement [m]
f	Fanning friction factor [-]
h	Heat transfer coefficient [$\text{W}/(\text{m}^2\text{K})$]
m	Mass [kg]
\dot{m}	Mass flow rate [kg/s]
p	Pressure [bar]
t	Time [s]
v	Velocity [m/s]
A	Area [m^2]
C_1	Pressure drop calibration coefficient [-]
C_d	Discharge coefficient [-]
D	Diameter [m]
H	Specific enthalpy [kJ/kg]
L	Length [m]
Nu	Nusselt number [-]
Pr	Prandtl number [-]
R	Radius [m]
R_a	Surface roughness [μm]
Re	Reynolds number [-]
T	Temperature [$^{\circ}\text{C}$]

subscripts

b	bubble
wl	wall
wf	working fluid
o	total
∞	boundaries

Acronyms

CBV	Compressor By-pass Valve
CGT	Compressor-Generator-Turbine
EXTV	Inventory Extraction Valve
GWP	Global Warming Potential
HP	High Pressure
INJV	Inventory Injection Valve
LP	Low Pressure
ODP	Ozone Depletion Potential
PCHE	Printed Circuit Heat Exchanger
PHE	Plate Heat Exchanger
PHX	Primary heat exchanger
PI	Proportional-Integral
sCO ₂	Supercritical carbon dioxide
TBV	Turbine By-pass Valve
SS 316L	Stainless steel 316L
TBV	Turbine By-pass Valve
WHR	Waste Heat Recovery

safe operating region, different methods have been proposed, such as regulation of the heat sink conditions [6] or the action on the flow split ratio between compressor and recompressor [7]. For the turbine, the use of throttling or by-pass valves is being considered [8,9].

Alongside turbomachinery bypass and throttling, inventory control is a key strategy to modulate the power output of sCO₂ power systems to enhance their flexibility [9], i.e. their ability to promptly and efficiently

adapt to variations in operating conditions imposed by the heat source (e.g. industrial manufacturing process), the heat sink (environmental factors) or the grid (demand variability, volatility of renewable energy sources in the power mix).

Such advantages have been demonstrated by Refs. [9,10], whose research concerned the development of mixed control strategies involving a conjunct use of by-pass, throttling and inventory control to

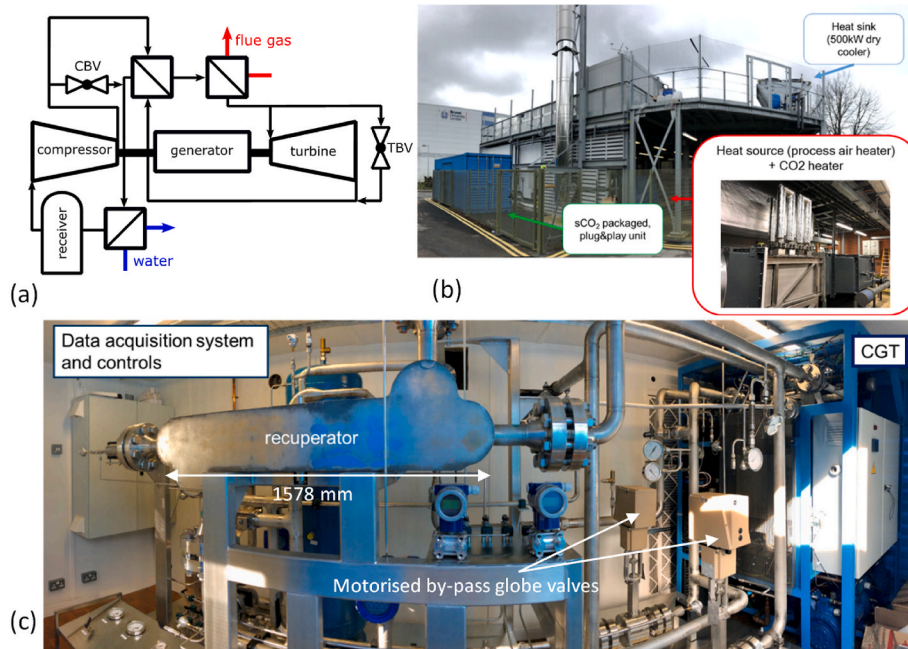


Fig. 1. sCO₂ facility at Brunel University London: (a) system layout, (b) facility overview, (c) sCO₂ loop inside the blue container shown in (b). (For interpretation of the references to colour in this figure legend, the reader is referred to the Web version of this article.)

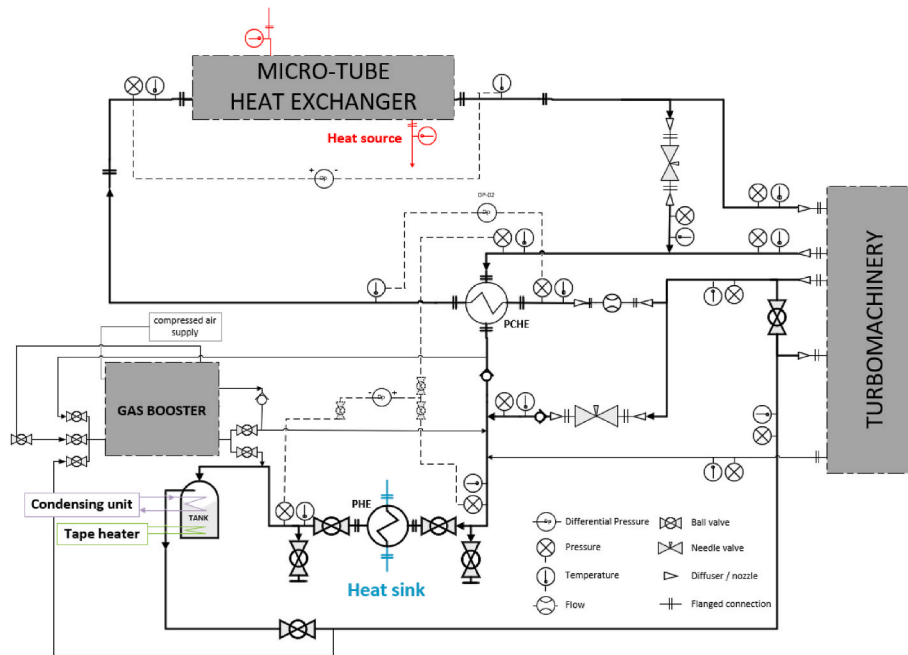


Fig. 2. Simplified P&ID of the sCO₂ facility at Brunel University London (Adapted from Ref. [16]).

follow the generator load of a sCO₂ recompression power unit for nuclear applications. The author in Ref. [11] presented different inventory control schemes and compared them in terms of response time and effectiveness. This included the adoption of a single inventory tank connected to both the low- and high-pressure side of the circuit or the use of multiple tanks connected to different charging/discharging points. However, stability implications (e.g. pressure gradients in the loop) due to the withdrawals/additions of CO₂ and the implications of having finite storage capacity in the inventory storage tanks have not been adequately considered in the literature.

To fill the literature gap, this research advances the state of the art through a numerical assessment of the effects of inventory control on the dynamic response of a small-scale sCO₂ heat to power system. A unique feature of this study is the modelling methodology that combines the dynamics of the sCO₂ heat to power unit (calibrated against real equipment data) with those of the inventory control system using finite capacity tanks. Insights on the dynamic behaviour of the inventory system to support the design and thermal management of the CO₂ storage tanks are provided. A Proportional Integral (PI) inventory controller has been designed to regulate the turbine inlet temperature following variations of the waste heat loads. Its response and effect on system performance and main cycle parameters are then analysed and discussed.

2. System description

The modelled sCO₂ system refers to a plug and play 50 kWe sCO₂ unit for Waste Heat Recovery (WHR) applications available at Brunel University London. The sCO₂ facility in Fig. 1 is based on a simple regenerative Joule-Brayton cycle (Fig. 1a) and it is equipped with three heat exchanger technologies: a micro-tube gas/sCO₂ heat exchanger for direct heat recovery from the heat source; a Printed Circuit Heat Exchanger (PCHE) employed as recuperator; and a Plate Heat Exchanger (PHE) as gas cooler. PCHEs are commonly used in the oil and gas sector because of their reliability in operating at high pressures and temperatures [12]. For this reason, they have also been adopted in sCO₂ power applications [13] as recuperators and also gas coolers [14]. For the Brunel test facility a plate heat exchanger (PHE) has been selected as gas cooler to reduce cost. This is of paramount importance in WHR

applications.

Other components include a radial turbine, a radial compressor and a synchronous brushless generator/motor mounted on the same single shaft, and motorised compressor and turbine by-pass globe valves (CBV and TBV respectively shown in Fig. 1a and 1c) to control the system at nominal, startup, shutdown and emergency operations. The CBV valve is located between the compressor outlet and gas cooler inlet while TBV is placed between the turbine inlet and outlet (Fig. 1c). All such components are packaged in a standard 20 ft container (Fig. 1c) except for the micro-tube heat exchanger, also known as primary heater, which is located along the exhaust line of the Process Air Heater (Fig. 1b). The Process Air Heater simulates the industrial waste heat source and provides flue gases up to 1.0 kg/s and temperatures up to 800 °C. The facility is also equipped with a 500 kW dry cooler system that rejects heat from the gas cooler to the ambient. Variable speed drives for the water pump and fans of the dry cooler allow variation of heat removal from the gas cooler.

A data acquisition and control system has been also installed (left-hand side of Fig. 1c) to enable remote control and monitoring of the unit. Two 10-m pipes connect the loop packaged in the container to the primary heater, which has been specifically designed to enhance the gas/sCO₂ heat transfer without causing an excessive pressure drop on the flue gas side. The sCO₂ test facility has been designed for small scale waste heat recovery applications (with an estimated net power output in the range of 50–75 kWe at design conditions). At these operating conditions, the turbomachinery impellers become very small and high speed which impacts negatively on their efficiency. Another challenge of small-scale sCO₂ systems is the cost per kilowatt installed. Their capital expenditure (CAPEX) is not linear with the power size especially in the case of the heat exchangers, which typically are responsible for the majority of the equipment budget [14,15].

Unless costs are significantly reduced, sCO₂ technology is primarily competitive for applications beyond 1 MWe power output and heat-source temperatures above 350 °C. Despite the low power output, this pilot scale research is expected to advance the knowledge in the field of sCO₂ power research and further support the uptake of sCO₂ technology. Furthermore, as reported in Ref. [17] sCO₂ turbomachinery will still have to be radial as long as the system power output stays below 12 MWe. For these reasons, the analysis reported in the following sections

Table 1

– Summary of transducers accuracies [16].

Accuracy	High	Standard
High pressure transducers	0.17 bar	0.52 bar
Low pressure transducers	0.10 bar	0.34 bar
Temperature transducers (RTD)	0.03 K	0.06 K
DP transducers	1.9 mbar	
Mass flow rate (Coriolis)	0.35% of measured value	

Table 2

– Estimated measurement uncertainty at design conditions [16].

Uncertainty	Power	Efficiency
Compressor	2.66%	3.32%
Turbine	0.43%	0.47%
Heater	0.36%	
Recuperator (cold/hot side)	0.36%/0.35%	
Cooler	0.61%	

should be transposable to the design and operation of full-scale sCO₂ power systems. Further details on Brunel's high-temperature heat to power conversion (HT2C) facility are available in Ref. [18]. Fig. 2 shows a simplified P&ID of the facility detailing in particular the location of pressure, temperature and mass flow rate sensors in the unit. Tables 1 and 2 detail the sensors installed and the estimated uncertainty of efficiencies and power for each system component.

3. Modelling methodology

The model of the sCO₂ heat to power conversion system has been developed in the commercial software GT-SUITE™. This tool is based on a one-dimensional (1D) formulation of Navier-Stokes equations and on a staggered grid spatial discretization [19]. Each component can be independently modelled through input data relating to geometrical features as well as their performance.

The components modelled as equivalent 1D objects are heat exchangers and pipes while the turbomachines, valves and the receiver are treated with a lumped approach. The 1D models discretise the components into a series of capacities such that manifolds are represented by single volumes while pipes are divided into one or more volumes. These volumes are connected by boundaries. The scalar variables (pressure, temperature, density, internal energy, enthalpy, etc.) are assumed to be uniform in each volume. On the other hand, vector variables (mass flux, velocity, mass fraction fluxes, etc.) are calculated for each boundary [19]. Each capacity considers the algebraic sum of all the incoming and outgoing mass flow rate contributions occurring at the boundaries (B), as per the continuity equation (1).

$$\frac{dm}{dt} = \sum_{i=1}^B \dot{m}_i \quad (1)$$

The pressure dynamics in the system is calculated through the momentum equation (2), which neglects body forces and considers the algebraic sum of momentums through the boundaries, pressure forces and dissipations due to friction and pressure drops [19]. In pipes, the latter two terms are respectively related to distributed (i.e. due to surface roughness) or concentrated (i.e. due to bends) pressure losses.

$$\frac{d(\dot{m}v)}{dt} = \frac{1}{dx} \left(dpA + \sum_{i=1}^B (\dot{m}v)_i - 4f \frac{\rho v |v|}{2} \frac{dxA}{D} - \xi \left(\frac{\rho v |v|}{2} \right) A \right) \quad (2)$$

The energy equation (3) is expressed in terms of total enthalpy. This formulation is required for the further implicit integration scheme employed by the solver for the analysis of energy systems whereas resolving fast dynamics (e.g. indicating pressure in positive displacement machines) is not the end goal [19]. Neglecting variations of

Table 3

Heat exchangers specifics.

Flow parameters		PHX	PCHE	PHE
Nominal heat duty	kW	388.3	630.0	237.5
Nominal UA value	kW/K	1.3	20.3	16.8
Hot side pressure drop	kPa	1.1	128.0	8.7
Cold side pressure drop	kPa	64.0	120.0	89.1
Geometrical features				
Heat transfer surface	m ²	3.92	12.00	6.21
Hydraulic diameter	mm	2.00	1.22	
Dry weight	kg	305.0	305.0	52.4
Material	–	Inconel 718	SS 316L	
Model details				
Time constant	s	1.55	7.25	2.38
Channel sub-volumes	#	25	50	50

Table 4

Heat exchanger calibration data (Cal) and comparison with model interpolation (Int), Gnieliski (Gn) and Dittus-Boelter (DB) correlations.

		Re = 20,000		Re = 25,000		Re = 30,000	
		Nu	Err%	Nu	Err%	Nu	Err%
Heater	Cal	73.0	N/A	92.2	N/A	106.8	N/A
	Int	73.4	1.3	92.5	0.3	107.2	0.4
	Gn	75.7	2.7	90.9	1.4	101.9	4.8
	DB	80.1	8.7	96.5	4.4	108.6	1.6
Recuperator	Cal	596.2	N/A	767.6	N/A	876.9	N/A
	Int	596.2	0.0	756.8	1.4	878.1	0.1
	Gn	596.9	0.1	735.6	4.2	886.2	1.0
	DB	629.4	5.3	779.9	1.6	944.7	7.2
Cooler	Cal	371.5	N/A	464.0	N/A	560.1	N/A
	Int	373.4	0.5	454.6	2.1	554.5	1.0
	Gn	376.5	1.3	445.4	4.2	544.7	2.8
	DB	369.1	0.6	437.0	6.2	533.2	5.0

potential energy, for a given capacity, the rate of change of total enthalpy depends on the volume capacity variations, the enthalpy fluxes and the heat transfer phenomena. The solution of the energy equation requires the computation of the local heat transfer coefficient through calibrated heat transfer correlations.

$$\frac{d(\rho H_0 V)}{dt} = \sum_{i=1}^B (\dot{m} H_0)_i + V \frac{dp}{dt} - hA(T_{wf} - T_{wt}) \quad (3)$$

3.1. Heat exchangers

The properties of the equivalent 1D channels of heat exchangers are defined starting from the geometrical inputs of the component. The performance data, which refer to different operating conditions of the heat exchangers, are used to compute the best fitting coefficients of the Nusselt-Reynolds (Nu-Re) correlations along the equivalent 1D networks [19]. Such data are provided by the manufacturers or calculated from more complex models (e.g. 3D CFD).

Table 3 summarises the geometrical features of the PCHE recuperator as well as the number of sub-volumes in which the different heat exchangers have been discretized. Their time constants have been also reported, calculated as the ratio between the heat exchanger mass multiplied by the specific heat capacity (m^*cp) of the material and conductance (UA) of the heat exchanger. It can be seen that the primary heater (PHX) has the lowest thermal inertia and the recuperator the highest due to its much higher thermal mass of the material used for its manufacture.

The results of the regression analyses carried out to calibrate the several heat exchangers are detailed in Table 4, which compares the Re-Nu curve interpolation of the different data provided by the manufacturer against the ones obtained by using the Gnieliski [20] and Dittus-Boelter [21] heat transfer correlations. It can be observed that the Gnieliski correlation provides better predictions of the manufacturer

Table 5
Summary of the turbomachinery aerothermal design.

	Turbine	Compressor
Diameter	72 mm	55 mm
No. of blades (Rotor)	14	7
No. of blades (Nozzle)	17	11
Isentropic efficiency (total-to-static)	70%	76%

data. For this reason, in the absence of data on heat exchanger performance from experimental tests, the Gnieliski correlation for the calculation of the heat transfer coefficients was employed in this study [22]. The full modelling methodology is available at [22].

The pressure drops are computed using a modified version of the Colebrook relationship in Equation (4). In this expression, the Fanning factor is calculated using the explicit approximation of the Colebrook equation proposed by Serghides [23], which is valid for the turbulent regime ($Re_D > 2100$). The quantities C_2 and C_3 , which can be calculated using Equations (5) and (6), account for the roughness of the heat exchanger channels Ra . The term C_1 is the calibration coefficient used to adapt the simulation results to the performance data provided by the heat exchanger manufacturer.

Even though this modelling methodology is common to all the three heat exchangers considered, the gas cooler requires an additional correlation to account for possible condensation of CO_2 . In this case, to predict the phase change, the formation of vapor bubbles or liquid droplets is addressed by evaluating the fluid density in each sub volume, while the two-phase area is computed using the vapor Rayleigh-Plesset formulation in Equation (7) [24].

$$f = C_1 \left(\frac{1}{4} \left(4.781 - \frac{(C_2 - 4.781)^2}{C_3 - 2C_2 + 4.781} \right)^{-2} \right) \quad (4)$$

$$C_2 = -2.0 \log_{10} \left(\frac{Ra/D}{3.7} + \frac{12}{Re_D} \right) \quad (5)$$

$$C_3 = -2.0 \log_{10} \left(\frac{Ra/D}{3.7} + \frac{2.51C_2}{Re_D} \right) \quad (6)$$

$$\frac{p_b - p_\infty}{\rho} = R \frac{d^2 R}{dt^2} + \frac{3}{2} \left(\frac{dR}{dt} \right)^2 + \frac{4\nu}{R} \frac{dR}{dt} + \frac{2\sigma}{\rho R} \quad (7)$$

3.2. Turbomachines

The turbomachines have been modelled as lumped components by using performance maps. The performance maps use the boundary conditions (temperature/pressure and shaft speed) to evaluate the performance of the machine and outlet conditions. The advantage of modelling the turbomachinery with performance maps is that it allows faster calculation results as the model is reduced order and also the dynamics of turbomachinery is relatively faster compared to the heat exchangers and other components with higher volume and high thermal inertia. Their aerothermal design is detailed in Table 5. Performance maps have been calculated by performing 3D RANS CFD simulations whose modelling methodology has been discussed in Refs. [25,26,27]. The 3D modelling approach has been validated through experimental data available from the Sandia National Laboratories [28], with an uncertainty lower than 5% [26,27]. The inlet boundary conditions of the 3D model are the total pressure and temperature as well as the flow direction, which is considered normal to the boundary. Outlet average static pressure has been chosen as outlet boundary condition.

The turbine operating and isentropic efficiency maps have been expressed through reduced quantities (pressure ratio versus reduced mass flow rates and reduced revolution speed) in order to account the variation of turbine performance on a change of the inlet conditions. Representation of turbine maps can be also found in Ref. [22].

Although this approach is fine for the turbine, which operates in a region where the CO_2 behaviour can be considered similar to the one of an ideal gas, this does not hold for the compressor, which operates near the fluid critical condition. Furthermore, the use of maps based on reduced quantities for the compressor leads to numerical instabilities when dealing with the inventory control action.

Therefore, the compressor map has been condensed to one curve

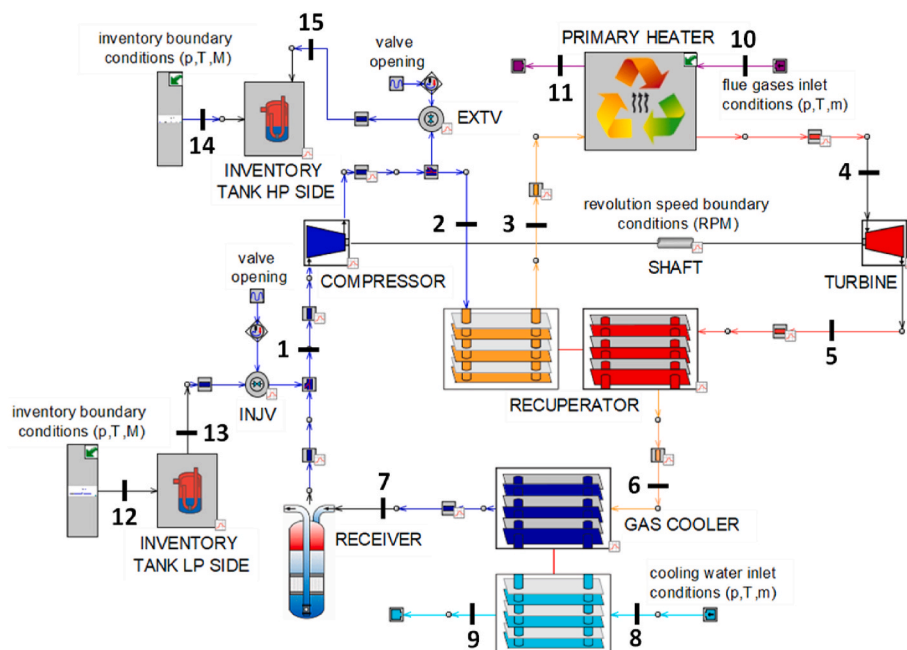


Fig. 3. Model diagram of the full CO_2 heat to power conversion block including inventory system.

using non-dimensional parameters, following the approach detailed in Ref. [29]. This allowed to solve numerical instabilities following the simulation of the inventory control action and to better account the effect of variable compressor inlet conditions on its performance. The inertia of the shaft has been modelled but the electrical machine characteristics have not been covered in scope of current work. The losses and consumptions of auxiliary equipment for turbomachinery lubrication and cooling have also been neglected.

3.3. Valves and other equipment

The valves have been modelled as orifices with variable area. A lookup table provides a series of forward and reverse discharge coefficients as a function of the lift position of the valve actuator. Such data have been retrieved by the manufacturer of the needle valves [30], which have been designed to follow an equal percentage characteristic curve. These discharge coefficients are then used to compute the effective flow area at the throat, while the pressure ratio across the valves allows to calculate the velocity at the throat. The velocity multiplied by the fluid density and the throat flow area gives then the mass flow rate passing through the valve. Equation (8) shows the correlation relating the valve discharge coefficient to the ratio between the actuator lift L and the valve diameter D [30].

$$C_d = 0.0112e^{0.196\frac{L}{D}} \quad (8)$$

The 1D modelling approach used to simulate heat exchanger behaviour has been adopted as well for straight pipes and bends. Bends introduce concentrated pressure drops while pipes have been considered as smooth and insulated, which means thermal losses are neglected. This assumption is reasonable based on the relatively large value of pipe diameters used in the Brunel sCO₂ test facility to minimise pressure drop as well as their insulation with ceramic wool layer wrapped between an inner layer of silica wash treated glass cloth and an outer layer of grey PTFE coated glass cloth to reduce heat losses.

The receiver, situated downstream the gas cooler (Fig. 2) to absorb the thermal expansion of the fluid in the circuit, has been modelled as a container (capacity) with fixed volume. Its volume is 0.165 m³ and accounts for almost 50% of the overall system capacity.

3.4. Inventory system

The inventory control system considers two tanks, modelled as finite volumes, whose value can be set as inputs to the model. The arrangement of the two tanks is shown in the schematic representation of the system in Fig. 3. The inventory tank connected downstream of the compressor (on the high pressure, HP, side of the circuit, point 15 in Fig. 3) has always a pressure lower than the one on the discharging point on the circuit (point 2, Fig. 3). Such pressure difference between the tank and the loop drives the withdrawal and storage of the working fluid from the loop to the tank respectively. The variable opening of a valve (namely the extraction valve, EXTV) allows to regulate the amount of fluid flowing from the loop to the tank. The other inventory tank connected upstream of the compressor (on the low pressure, LP, side of the circuit, point 1 in Fig. 3) enables the injection of additional CO₂ to the loop. In this case, to drive the fluid injection from the tank to the loop, the tank pressure (point 13, Fig. 3) is higher than the one at the charging point (point 1, Fig. 3). Another valve (namely the injection valve, INJV) can be actuated to regulate the fluid injection into the circuit.

Both valves are modelled as orifices as detailed in the previous section. The inventory tank sub-models require as boundary conditions the tank volume, the initial tank fluid temperature and initial pressure. An initialization process starts then, based on these three variables, the initial mass of fluid in the tanks at the beginning of the simulation (point 12 and 14, Fig. 3).

Fig. 3 also shows the general model boundary conditions required for

Table 6

Nominal operating conditions and performance of the sCO₂ heat to power conversion loop.

Supercritical CO ₂		Design	Model I/O
Mass flow rate	kg/s	2.2	Output
Highest pressure	bar	137.5	Output
Lowest pressure	bar	75.0	Output
Highest temperature	°C	465	Output
Lowest temperature	°C	33	Output
Heat source: flue gas			
Mass flow rate	kg/s	1.0	Input
Inlet temperature	°C	650	Input
Inlet pressure	bar	1.0	Input
Cold source: Water			
Mass flow rate	kg/s	1.6	Input
Inlet temperature	°C	15	Input
Inlet pressure	bar	3.0	Input
sCO ₂ unit			
Net thermal power output	kW	75	Output
Overall efficiency	%	24	Output
Turbomachinery speed	RPM	86,000	Input
Mass charge	kg	61	Input

the simulations, which are indicated with lower case letters. These boundary conditions are the revolution speed of the compressor-generator-turbine unit along with the inlet temperatures, pressures and mass flow rates of the hot and cold sources. The thermodynamic properties of the fluids are computed using an interface between the solver and the NIST database [31].

4. Inventory tank assessment

To broadly assess the impact of potential inventory control actions on the main thermodynamic variables of the tanks and the loop, the injection and the withdrawal of CO₂ into and from the circuit has been simulated assuming different inventory tank initial pressures and volumes. For each of the simulations the inlet conditions of the heat source and sink as well as the revolution speed of the turbomachines has been kept constant and equal to the nominal values (Table 6).

A pre-defined opening profile for the EXTV and INJV valves has been set and maintained constant for all the simulations. Such opening profile has been selected considering a valve opening time required to allow the achievement of steady-state conditions in the loop and in the tanks after the CO₂ injection/withdrawal actions are performed.

4.1. Inventory tank dynamics

Fig. 4 shows the inventory tank dynamics following the injection and withdrawal of CO₂ in the loop assuming an inventory tank capacity equal to the one of power loop (0.243 m³). Each different initial tank pressure is represented by a different line. The range of pressures analysed varies from 82.5 bar up to 112.5 bar for both inventory tanks. The initial mass and temperature levels of the CO₂ in the tanks are correlated to the initial pressure and tank capacity considered (Table 7) across a range between 88 and 152 kg and 38–45 °C respectively.

Fig. 4a-c shows the pressure, temperature and mass transient profiles of the inventory tank connected to the low-pressure side of the system after the INJV valve opening. During the 50s transient, the CO₂ stored in the tank is injected into the loop, causing an expansion and thus cooling the gas contained in the tank. The temperature does not fall below the critical point, eliminating the risk of condensation (Fig. 4b). However, more detailed numerical simulations or experimental analyses may be required to assess local heat transfer phenomena and potential risks of blowdown, at least in the most extreme cases where the pressure of the CO₂ goes from 112.5 bar down to 89 bar with a resulting temperature drop of 8 °C (Fig. 4b and 4 c).

Symmetric trends can be observed during the extraction of fluid from the CO₂ loop to inventory tanks connected to the high-pressure side of

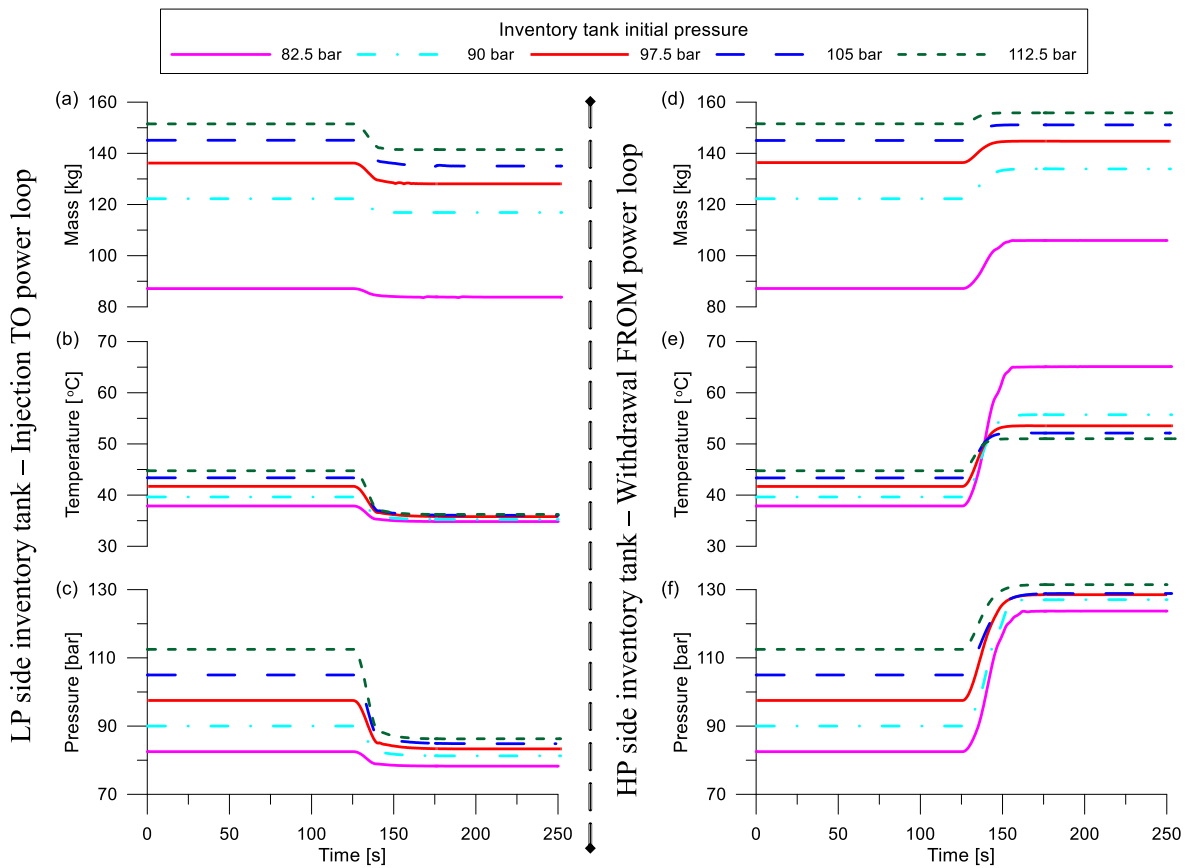


Fig. 4. Effects on tank mass (a), temperature (b) and pressure (c) following the injection of CO₂ into the power loop (left-hand side) or an extraction of CO₂ from the power loop (right-hand side) for a tank volume equal to the one of the loop.

Table 7
Main simulation parameters of inventory system.

Initial conditions at both inventory tanks		Min	Max
Pressure (Model input)	bar	82.5	112.5
Volume (Model input)	m ³	0.073	0.729
Temperature (Model output)	°C	38	45
Mass (Model output)	kg	88	152

the loop (downstream the compressor, Fig. 4d-f). The only slight difference can be noticed in the temperature profiles, where the larger temperature variation, from 38 °C to 65 °C, occurs when the initial pressure level of the HP side tank is set to 82.5 bar. In this case, the mass of CO₂ contained in the vessel is lower compared to the other cases, and therefore the stream of CO₂ flowing at higher temperature from downstream the compressor has a higher impact in warming up the tank (Fig. 4e).

The results also show that both the injection and withdrawal processes cannot be considered isothermal, given the relevant temperature variations occurring during the fluid expansion (CO₂ injection) and during the fluid compression in the tank following mixing with the higher temperature and pressure CO₂ stream flowing from the loop (CO₂ extraction). This assumption in the sizing stage of the tanks could lead to errors in the predictions of the control action outcomes, given the high dependency of the thermophysical properties of CO₂ on pressure and temperature changes.

Fig. 4a and 4d shows the working principle of the inventory control action. Transferring part of the mass contained in the inventory tank to the CO₂ circuit (CO₂ injection, Fig. 4a) and vice versa (CO₂ withdrawal, Fig. 4d), enables the mass of CO₂ in the circuit to be altered in order to

adapt the system electric output to the grid load, but also, for a given heat load, decreasing/increasing the temperature at the turbine inlet. This effect is shown in Fig. 5.

In particular, Fig. 5 shows that injection of CO₂ into the loop leads to a decrease in the CO₂ turbine inlet temperature from the nominal level of 460 °C down to 414 °C, 381 °C, 372 °C, 363 °C and 350 °C for a LP side inventory tank initial pressure of 82.5 bar, 90.0 bar, 97.5 bar, 105.0 bar and 112.5 bar respectively. Lower initial tank pressures lead to lower injection of CO₂ mass into the system and therefore to higher turbine inlet temperatures. The opposite holds for the temperature at the compressor inlet (Fig. 5a), since in the same way, higher mass in the circuit for a given cooling load leads to higher temperature at the gas cooler outlet and therefore at the compressor inlet.

The compressor inlet pressure adapts to the tank pressure level when the initial tank pressure is equal to 82.5 bar, for higher initial pressure levels the equilibrium pressure in the loop achieves slightly lower values (from 84 bar to 89 bar, Fig. 5b). The pressure at the turbine inlet follows the same trend, rising from the nominal value of 132 bar–139 bar, 145 bar, 149 bar, 152 bar and 156 bar for increasing tank initial pressure levels (82.5 bar, 90 bar, 97.5 bar, 105 bar and 112.5 bar respectively).

Withdrawing CO₂ from the circuit, leads to a drop in the CO₂ pressure both at inlet to the compressor and turbine (Fig. 5d). It can also be noticed that large amount of fluid withdrawn, introduce small instabilities in lead to undesirable conditions for some system components (i.e. condensation occurring at the compressor inlet, Fig. 5c and 5d. Further investigations into best locations in the loop for charging/discharging may improve the system pressure response during such transient operating conditions.

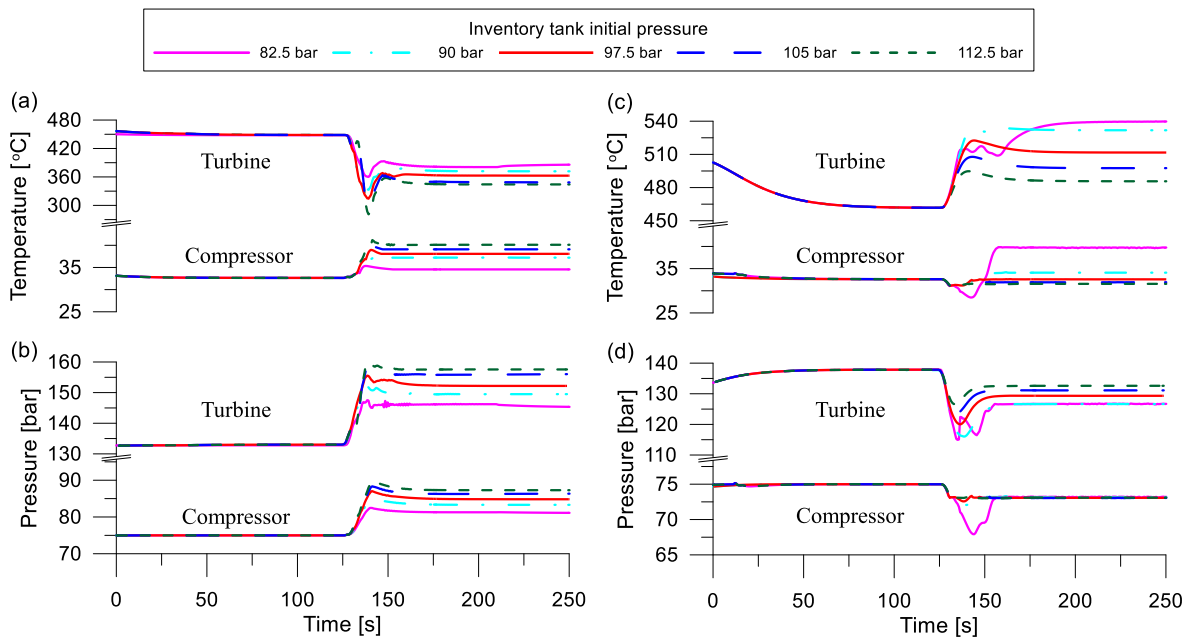


Fig. 5. Effects on compressor and turbine inlet temperature (a) and pressure (b) following the injection of CO₂ into the power loop (left-hand side figure) or an extraction of CO₂ from the power loop (right-hand side figure) for a tank volume equal to the one of the loop.

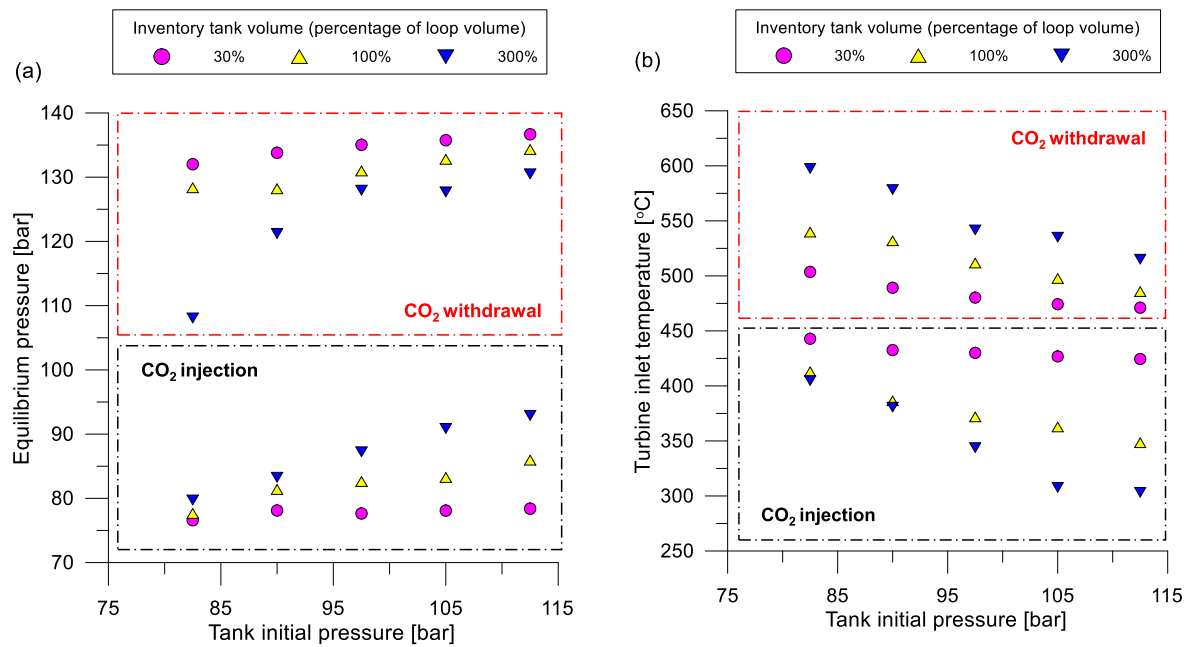


Fig. 6. Effects on system equilibrium pressure (a) and turbine inlet temperature (b) following the injection or withdrawal of fluid into and from the power loop for different inventory tank volumes (expressed as percentage of the loop capacity).

4.2. Inventory tank volume effect

The same analysis has been carried out considering different volumes for the inventory tanks. Fig. 6 a shows the pressure values achieved in the circuit after CO₂ injection/withdrawal considering inventory tanks with a volume (capacity) equal to 30%, 100% and 300% of the total loop one (including the receiver). The equilibrium pressure in the power loop gets closer to the initial pressure of the tank when its capacity increases, since for higher volume of the inventory tanks, the mass injected into the loop is higher. Such higher mass in the circuit also leads to the achievement of lower temperatures at turbine inlet, since the heat input from the waste heat source is kept constant during the simulation. For

instance, a turbine inlet temperature equal to 300 °C is achieved for a tank volume of 0.729 m³ and an initial pressure of 112.5 bar (Fig. 6b). Similar effects are also noticeable in case of CO₂ withdrawal from the power loop.

Higher tank volumes lead to an extended controllability range, e.g. lower temperatures achievable at the turbine inlet, and can ensure a more prolonged availability of the control action (slower tank discharging/charging). On the other hand, larger tank volumes would lead to challenging designs for the inventory tank thermal management system, because of the increased fluid thermal inertia. This is a challenging scenario, since the thermal management of inventory control tanks is among the possible solutions to restore the availability of the

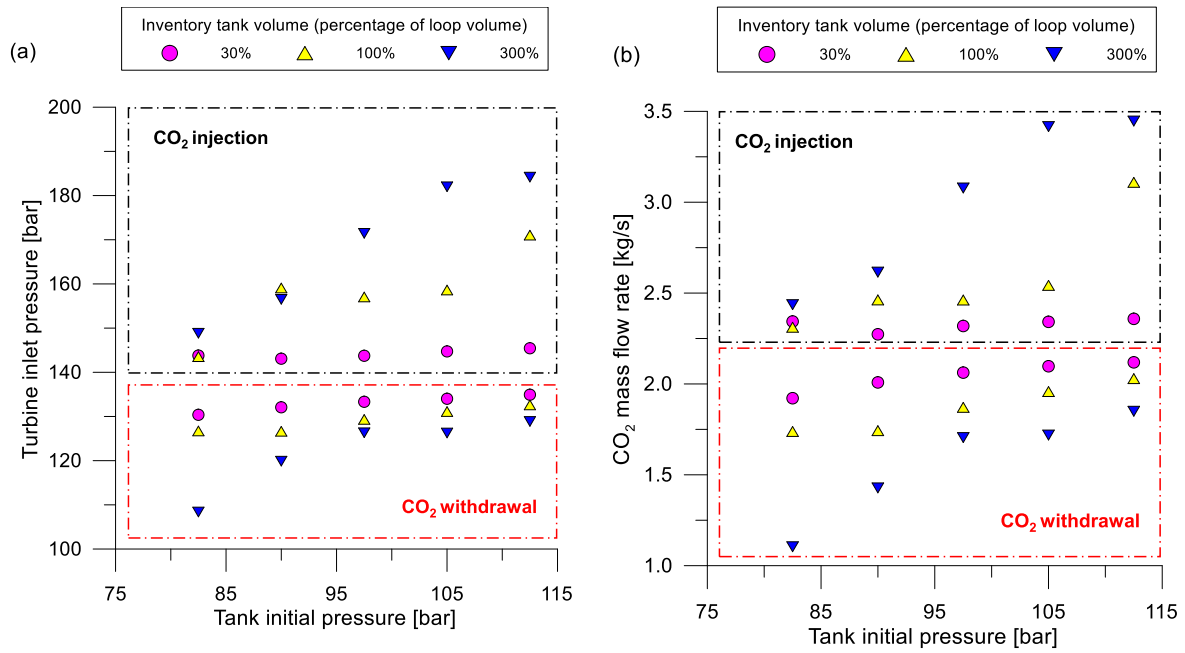


Fig. 7. Turbine inlet pressure (a) and CO₂ mass flow rate (b) following the injection or withdrawal of fluid into and from the power loop for different inventory tank volumes (expressed as percentage of the loop capacity).

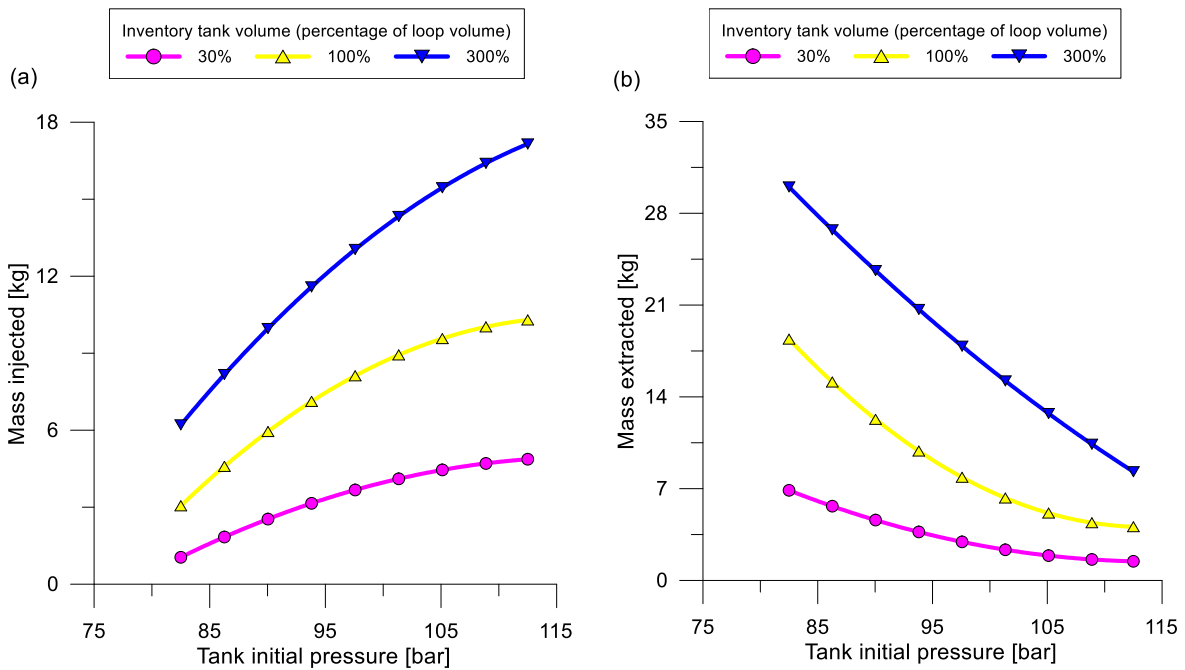


Fig. 8. Compressor inlet temperature as a function of pressure (a) and pressure (b) following the injection of CO₂ into the power loop (left-hand side figure) or an extraction of CO₂ from the power loop (right-hand side figure) for a tank volume equal to the one of the loop.

inventory controller after use (i.e. providing/removing heat to increase/decrease the tank pressure after usage). The adoption of large inventory tanks would then require auxiliary mechanical systems (i.e. additional pumps, gas booster and valves) to promptly restore the initial tank pressure level.

Fig. 7 shows that the same amplifying effects are noticeable on turbine inlet pressure (Fig. 7a) and on the CO₂ mass flow rate circulating in the power loop (Fig. 7b). In case of CO₂ injection, having a high capacity inventory tank leads to much higher level of mass in the circuit which increases substantially the pressure at inlet of the turbine (maximum

level of 180 bar for an inventory tank initial pressure and volume of 112.5 bar and 0.729 m³ respectively). The increased pressure level may overcome pressure design limits of the system, imposing constrains on the maximum mass of fluid injectable in the power loop.

In case of CO₂ withdrawal, having a large volume inventory tank (300% of power loop volume) allows to achieve larger decrease in system pressure level (minimum turbine pressure of 110 bar for a tank initial pressure of 82.5 bar, Fig. 7a) which may be a key feature for the implementation of less complex and more autonomous shutdown control strategies (isolating valves between low and high pressure side of

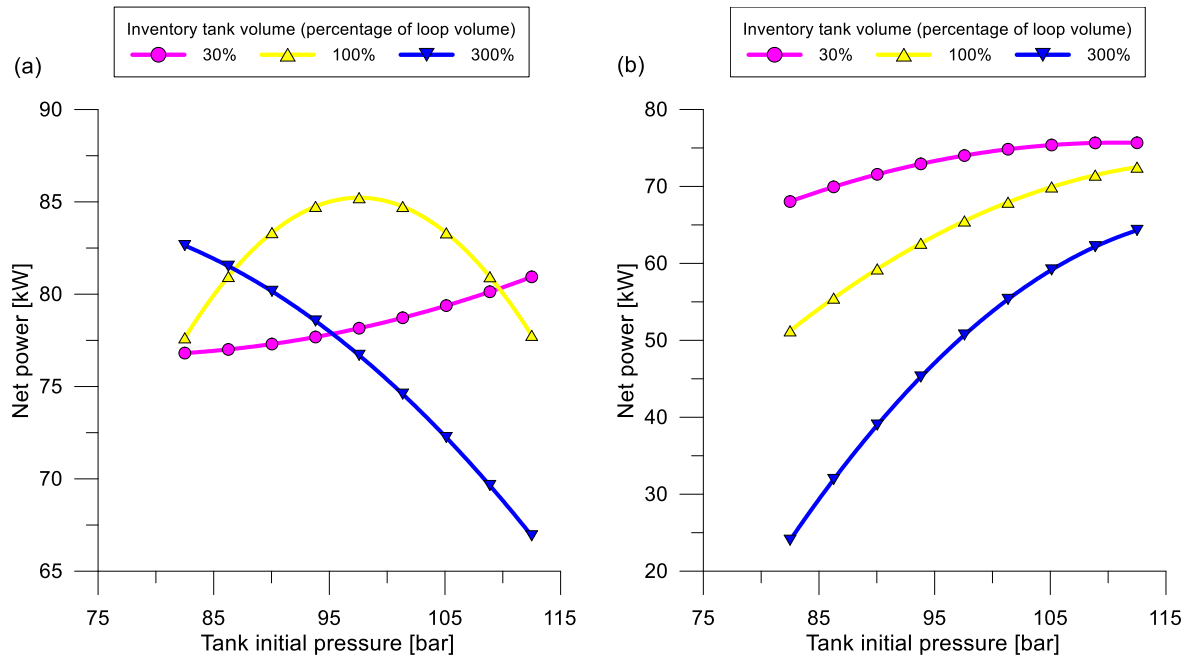


Fig. 9. Net power output of the system as a function of the inventory tank initial pressure level and volume following the injection of CO₂ into the power loop (a) or the extraction of CO₂ from the power loop (b).

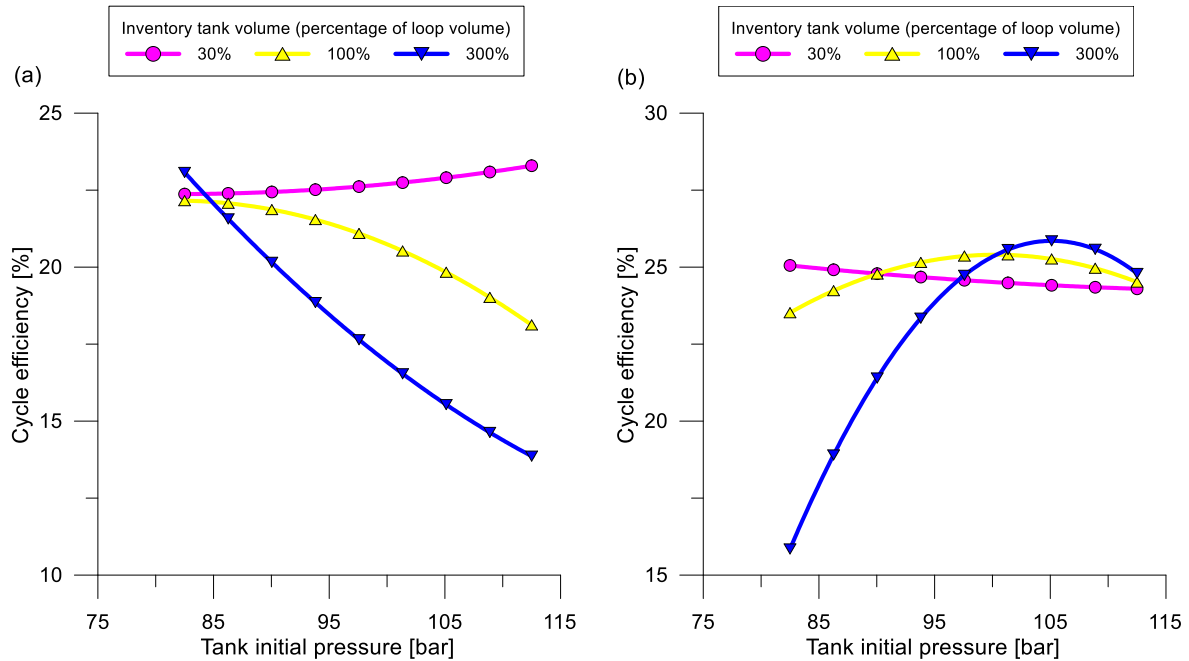


Fig. 10. Cycle efficiency of the system as a function of the inventory tank initial pressure level and volume following the injection of CO₂ into the power loop (a) or the extraction of CO₂ from the power loop (b).

the systems can indeed be avoided since the inventory control system can lower the equalizing cycle pressure in case of compressor shutdown).

CO₂ injection/withdrawal can substantially increase and decrease respectively the mass flow rate of CO₂ circulating in the loop (Fig. 7b), leading to a change also in the pressure drops across heat exchangers.

All the above effects are due to the increased or decreased level of fluid mass in the system, as showed in Fig. 8. Fig. 8 a shows the additional mass injected to the power loop for different initial pressure levels and inventory tank volumes while Fig. 8 b shows the mass removed from

the power loop. Increasing the capacity of inventory tank from 100% to 300% of the power loop volume can lead to an increase in injected fluid mass from 9 kg to almost 18 kg for an inventory tank initial pressure of 115 bar (Fig. 8a).

During the extraction, for the same volume increase, the removed mass from the power loop can vary from 19 kg to 31 kg for an initial pressure of the inventory tank of 82.5 bar (Fig. 8b). These results suggest that there is a difference among controllability ranges between CO₂ injection and extraction. Assuming same values for the initial pressure levels of both inventory tanks connected to the low- and high-pressure

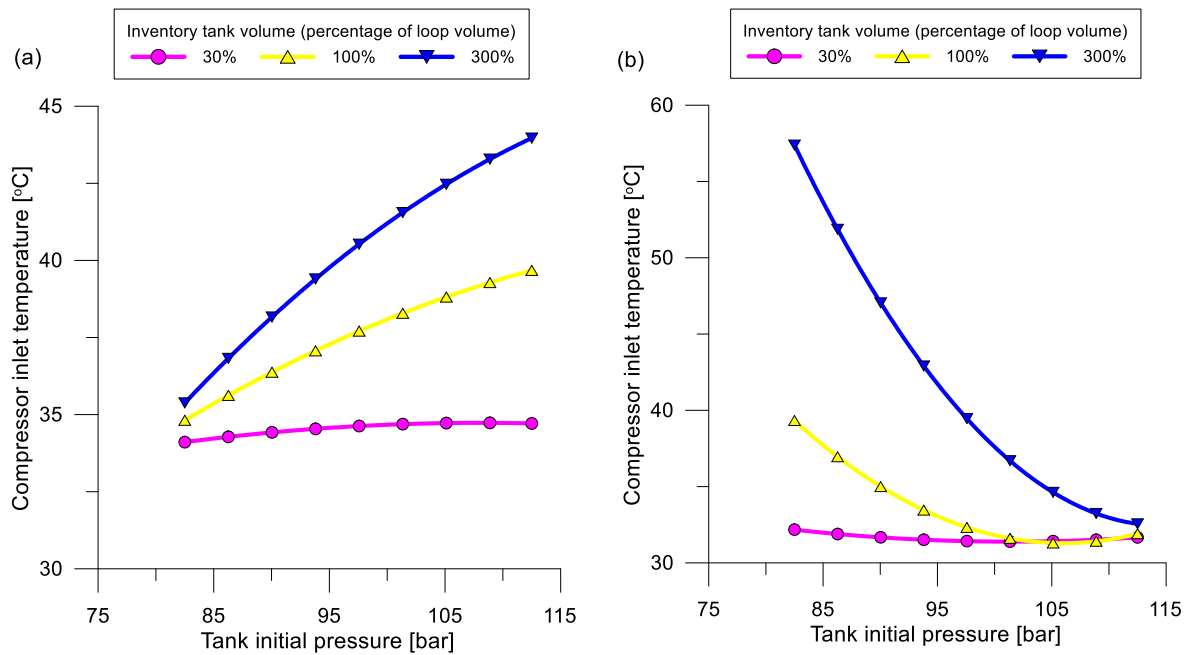


Fig. 11. Compressor inlet temperature as a function of pressure (a) and pressure (b) following the injection of CO₂ into the power loop (left-hand side figure) or an extraction of CO₂ from the power loop (right-hand side figure) for a tank volume equal to the one of the loop.

side of the circuit, leads to asymmetric pressure differences between inventory tank and extraction/injection points, with a consequent different effect of the control action. Therefore, inventory sizing should consider this aspect and assume different initial pressure levels for the tanks connected to the low- and high-pressure side of the system.

4.3. Inventory effect on system performance

Figs. 9 and 10 show the variation of system performance as a function of initial pressure and volume of the inventory tank following an injection and extraction of fluid. Fig. 9 reports the variation of system net power output and Fig. 10 the change in cycle efficiency. In particular, Fig. 9 shows the system net power output as the fluid is injected in the power loop. When the volume of the inventory tanks increases the mass injected in the loop for each initial pressure level increases as well, since more working fluid mass transfer is required to equalize the differential pressure between the tanks and the circuit. Small mass injections improve the system power output, because higher mass flow rates are circulating in the circuit. This allows to recover additional thermal power from flue gases without increasing excessively pressure drops across heat exchangers and changing excessively the thermodynamic conditions at turbine and compressor inlet as showed in Fig. 6 b, Fig. 7a and 11 a (whose efficiency then remain approximately constant).

Further additions of mass, however, can change significantly the thermodynamic conditions in the cycle and the CO₂ mass flow rate, which can impact negatively the efficiency of turbomachinery and the power generated by the power block. Simulation results showed the system power output drops to 77 kW and 66 kW for large amounts of CO₂ mass injected, occurring for a tank initial pressure of 112.5 bar and an inventory tank volume of 0.243 m³ and 0.729 m³ respectively (Fig. 9a).

There is then an optimal value of mass injected which maximises the power generated and it is different from the optimal charge that guarantees the system maximum thermal efficiency. Such condition, when the system is slightly overcharged occurs for a volume of the inventory tank equal to 0.243 m³ and an initial pressure level of 97.5 bar (Fig. 9a), corresponding to 8 kg of CO₂ mass injected (Fig. 8a).

CO₂ extraction from the power loop only decreases the system net

power output, as shown in Fig. 9 b. This is mainly due to the decrease of the turbine inlet pressure and the increase of the temperature at the compressor inlet (as showed in Fig. 11b) which leads to less efficient compression since the machine is operating far from the CO₂ critical point.

Similar trends can be observed from the system cycle efficiency results reported in Fig. 10, with the only exception occurring during fluid extraction. In Fig. 10 b it can be seen that the cycle efficiency slightly improves for small fluid extractions before decreasing substantially for larger removed amounts. Small reductions of fluid mass can lead to steeper drops in the heat recovered rather than on system net power output, causing the efficiency to increase. It can also be seen that the optimal charge for maximum efficiency may be different from the one required to achieve maximum power output.

5. Inventory control simulations

After the analysis of the effects of inventory main parameters on system variables and performance, an inventory controller was designed to regulate the temperature at the turbine inlet. The temperature at the inlet of the turbine is a crucial parameter to avoid critical thermal stresses on system components and ensure a safe operation of the system and turbomachine auxiliaries (i.e. sealing, bearings) during transients. Because the sCO₂ facility has been designed for waste heat recovery applications, the objective is to assess the controller response to a heat load variation. In this study in particular, the case of a heat load drop and increase have been simulated by considering a decrease and increase respectively of the flue gas inlet temperature.

The controller is a Proportional Integral (PI) one acting on the valve actuator lift position. Two such controllers have been connected to the inventory extraction and injection valves (EXTV and INJV respectively, Fig. 3). The controller on the EXTV, which connects one inventory tank to the high-pressure side of the power loop (downstream the compressor, point 2 in Fig. 3), is activated by a state machine controller when the primary heater sees a decrease in the heat load provided by the flue gases (which may occur for a temperature or flow rate decrease). In such case, fluid mass is removed from the power loop to counterbalance the decrease in thermal energy available.

Table 8

Proportional (P) and integral (I) coefficients for controllers acting on the extraction valve (EXTV) and the injection valve (INJV).

Controller coefficients		EXTV	INJV
P coefficient	[-]	0.31	-0.37
I coefficient	[-]	0.09	-0.07
Settling time	[s]	21	
Damping ratio	[-]	0.8	

On the contrary, the controller on the INJV, which connects the other inventory tank to the low-pressure side of the power loop (upstream the compressor, point 1 in Fig. 3), is activated by the state machine following a rise in heat source temperature or mass flow rate. Higher thermal energy is therefore balanced by an increase in the mass of fluid in the power loop. The state machine is thus regulated depending on the difference between the actual and the nominal level of temperature or mass flow rate of the heat source. If the difference is positive, means that the heat load provided by the flue gas is higher and then the controller acting on the INJV is activated. If the difference is negative, the controller on the EXTV is used.

A lambda tuning procedure has been used to calculate the proportional (P) and integral (I) terms of the controllers [32]. By considering a first order relationship between the mass injected/extracted into/from the power loop and the controlled process variable (turbine inlet temperature), the control output (valve actuator lift) has been modified in the entire admissible range and the process variable response analysed. From the time constant (τ) and process gain (K), the proportional and integral coefficients of the two controllers have been retrieved by setting

an appropriate settling time and damping ratio to smooth the controller response. Table 8 reports PI values for the two controllers with the respective settling time and damping ratio. In the following sections the controller performance and response are discussed in relation to a simulated decrease and increase of the heat load.

5.1. Heat load decrease

Fig. 12 shows the results of the system uncontrolled and controlled responses to a decrease in the heat load provided by the waste heat source, simulated through a decrease of 10% in the inlet temperature, from 650 °C down to 580 °C (grey continuous line, Fig. 12a). The temperature control set point (dashed red line in Fig. 12a) at the turbine inlet has been set equal to the turbine nominal temperature of 465 °C. The inventory tank volume was assumed equal to 0.243 m³ (same for the power loop), while its initial pressure has been set to 82.5 bar. Without control action, the turbine inlet temperature decreases from 465 °C to 400 °C, leading to a 65 °C temperature drop in approximately 50s. Turbine pressure, compressor inlet conditions, and mass flow rate remain on the contrary unchanged (Fig. 12a, c and d). Once the inventory control system is active, the regulation of the turbine temperatures is effective and the reference set point is achieved thanks to the removal of 11 kg of fluid mass from the power loop (dark brown continuous line in Fig. 12b).

As a result of the mass removal, the turbine and compressor inlet pressures decrease from the nominal value of 137.5 bar and 75 bar down to 126 bar and 72 bar respectively (blue and light brown line respectively in Fig. 12c). The mass flow rate also decreases from the nominal value of 2.2 kg/s down to 1.8 kg/s (pastel blue line in Fig. 12d). This is a

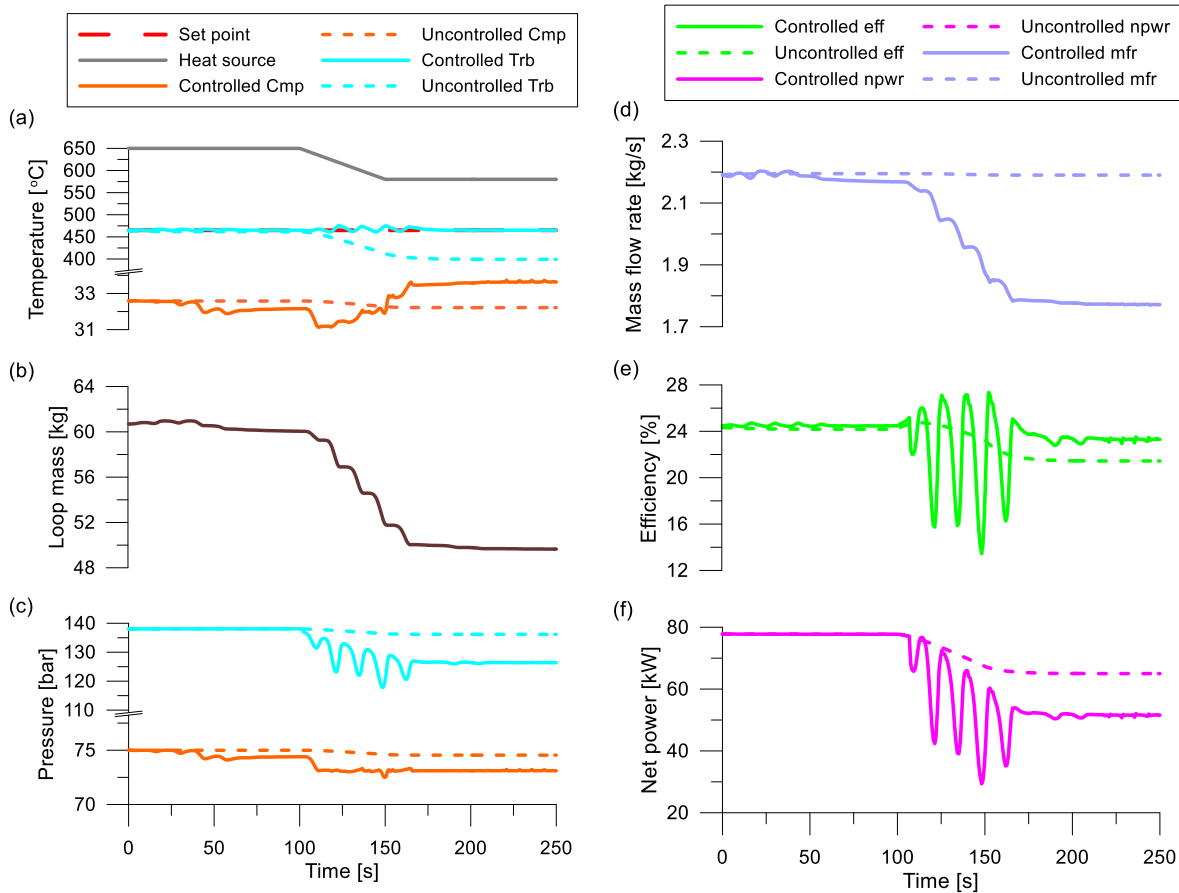


Fig. 12. Controlled and uncontrolled system response to a decrease in the heat source (hs) temperature: (a) set point, compressor (cmp) and turbine (trb) inlet temperatures; (b) mass in the power loop; (c) compressor and turbine inlet pressures; (d) CO₂ mass flow rate (mfr); (e) cycle efficiency (eff); (f) net power output (npwr).

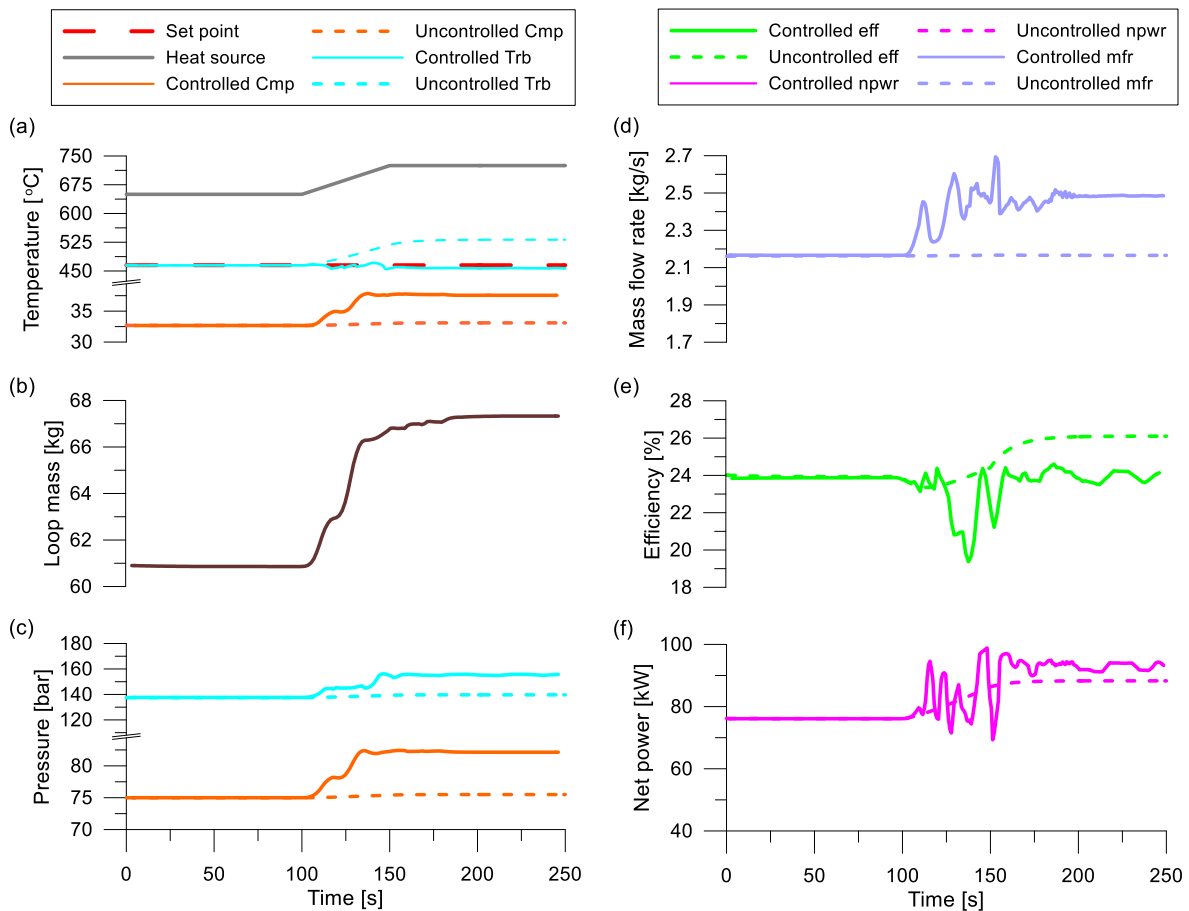


Fig. 13. Controlled and uncontrolled system response to an increase in the heat source (hs) temperature: (a) set point, compressor (cmp) and turbine (trb) inlet temperatures; (b) mass in the power loop; (c) compressor and turbine inlet pressures; (d) CO₂ mass flow rate (mfr); (e) cycle efficiency (eff); (f) net power output (npwr).

consequence of the reduced pressure ratio across the cycle induced by the lower fluid mass in the circuit, which changes the characteristic of the loop and reduces the mass flow provided by the compressor.

The removal of CO₂ from the power loop causes the compressor to operate close to the surge region, with oscillations at the outlet pressure which consequently result in oscillation in all the cycle calculated quantities, from the mass flow rate to the efficiency and net power output. More detailed analyses of the compressor operations (both numerical and experimental) would be required in future work to understand if an anti-surge valve can help to overcome the issue.

Fig. 12e and f show the effect of the inventory control action on the system performance. In particular the cycle efficiency is showed in Fig. 12e while the system net power output in Fig. 12f. The decrease in heat load has a detrimental effect on both efficiency and net power output. When the control system is not considered the efficiency of the cycle drops from 24% down to 22% (dark green line in Fig. 12e) following a decrease in the heat source temperature. The thermal power recovered from the flue gases stays the same, but the net power decreases from 78 kW to 65 kW (purple line in Fig. 12f).

The action of the inventory controller despite leading to a lower net power output of 52 kW (magenta line in Fig. 12f), 20% lower compared to the uncontrolled system, allows to achieve a higher cycle efficiency after the heat source temperature decrease (light green line in Fig. 12e). The less mass of fluid in the power loop indeed leads to a lower power production, but also to a much lower waste heat recovered compared to the uncontrolled system case, allowing to maintain a constant efficiency in part load conditions. Such results suggest that inventory control strategies for regulating the power unit in part-load conditions should be

preferred in power generation applications rather than waste heat recovery, where the net power generated has a higher value (since the heat source is a waste product).

5.2. Heat load increase

Fig. 13 shows system uncontrolled and controlled response for an increase of the heat load provided by the flue gases, simulated through an increase of 10% in the inlet temperature, which goes from the nominal value of 650 °C up to 725 °C (grey continuous line, Fig. 13a). In this case as well the temperature control set point has been kept equal to the turbine nominal temperature of 465 °C (Fig. 13a). The inventory initial pressure to 112.5 bar while the volume of the inventory tank has been set equal to 0.729 m³. Simulations adopting a volume of 0.243 m³, in fact, revealed the inability of the controller to achieve the target due to the saturation of control action. The available mass before the equalization of pressure between tank and power loop was not sufficient to cause an adequate drop in turbine inlet temperature.

When the system is not controlled, the turbine inlet temperature increases from 465 °C to 532 °C, leading also in this case to approximately 65 °C temperature difference in 50s. The pressure at the turbine and compressor inlet along with the compressor inlet temperature and CO₂ mass flow rate remains unchanged (Fig. 13a, c and d). The inventory controller instead even in this case is able to keep the turbine inlet temperature equal to the established set point (blue line in Fig. 13a) by adding 7 kg of fluid mass into the power loop (dark brown line in Fig. 13b). After the injection of the additional fluid mass, the pressure at turbine and compressor inlet increase from the nominal value of 137.5

bar and 75 bar up to 155 bar and 82 bar respectively (blue and light brown line respectively in Fig. 13c). The mass flow rate increases as well from the nominal value of 2.2 kg/s up to 2.5 kg/s (pastel line in Fig. 13d) following the increased cycle pressure ratio.

In this case, the inventory controller actually allows not only to promptly regulate the system but also to achieve better performance in terms of net power output, which goes from 77 kW up to 92 kW against the increase from 77 kW to 88 kW obtained in the uncontrolled case (Fig. 13f). In terms of cycle efficiency, Fig. 13 e shows that for an increase in the heat load the inventory controller allows to keep the system efficiency unchanged but lower compared to the one achieved by the uncontrolled power unit 26% when the waste heat source temperature achieves 725 °C (dark green light in Fig. 13e). Such results show that for increases of heat load provided by the waste heat source, the inventory controller is actually very effective also in optimizing system performance. Either in this case oscillating transients can be noticed due to the particular region of operation of the compressor.

6. Conclusions

This work provides insights on the dynamics of inventory control on a small scale sCO₂ heat to power conversion unit. The numerical methodology combines a one-dimensional CFD model of the sCO₂ power loop calibrated against real equipment data with a model of an inventory control system. The results show that, with respect to inventory design procedures available in the literature, the sizing of the inventory tanks cannot be carried out assuming CO₂ injection and withdrawal processes are isothermal. The simulations reported a maximum tank temperature change of 22% and 76% when the CO₂ is injected and withdrawn from the system respectively.

Such temperature change could lead to variation of fluid thermo-physical properties with consequent errors in the prediction of the control action outcomes. As inventory tank capacity is mainly related to the controllability range of the cycle, increasing the volume to 3 times that of the power loop led to ±30% variation in turbine inlet temperature compared to the nominal value. Larger tank volume could also lead to greater control flexibility but also to increased complexity in inventory thermal management, potentially requiring the use of mechanical systems (i.e. pumps, gas boosters, valves or multiple tanks) to restore the initial tank pressure level and therefore the control margin after multiple fluid injections/withdrawals to and from the power loop.

In general, even if the inventory controller can effectively regulate the turbine inlet temperature by injecting/withdrawing CO₂ into/from the power loop, such action influences several cycle parameters, with consequent complexity in predicting the outcome on system performance. For example, a decrease of 10% in the waste heat source temperature, the extraction of 11 kg of CO₂ mass from the power loop enacted by the PI inventory controller enables the turbine inlet temperature to remain constant at the nominal value of 465 °C but causes a 11 bar and a 2 bar reduction in the turbine and compressor inlet pressures respectively.

This combined with a decrease in CO₂ mass flow rate of 0.4 kg/s leads to a reduction in net power output of 13 kW but to an increase in efficiency of 2% compared to the performance of the uncontrolled system. Therefore, despite a small detrimental action on the power output, at part-load the controller is able to keep unchanged the cycle efficiency when the heat source temperature decreases. For a heat source temperature increase the controller is able to optimise the system net power output while keeping a constant cycle efficiency. Future work will be focused on assessing the relationship between mass injected/extracted and cycle performance as well as identifying strategies to improve transients occurring during the actuation of the control action.

Declaration of competing interest

The authors declare that they have no known competing financial

interests or personal relationships that could have appeared to influence the work reported in this paper.

Data availability

Data will be made available on request.

Acknowledgement

The research presented in this paper has received funding from the European Union's Horizon 2020 research and innovation program under grant agreement No. 680599 for the I-ThERM project. Funding for the work has also been received from the Research Councils UK, Grant No. EP/P004636 for the OPTEMIN project and Grant No. EP/V001795/1 for the SCOTWAHR project. The contribution from the funders and industry partners in these projects is gratefully acknowledged. Data related to the paper and other information relating to the paper can be obtained by contacting the corresponding author.

References

- [1] White MT, Bianchi G, Chai L, Tassou SA, Sayma AI. Review of supercritical CO₂ technologies and systems for power generation. *Appl Therm Eng* 2021;185. <https://doi.org/10.1016/j.applthermaleng.2020.116447>.
- [2] Marchionni M, Bianchi G, Tassou SA. Review of supercritical carbon dioxide (sCO₂) technologies for high-grade waste heat to power conversion. *SN Appl Sci* 2020;2: 611. <https://doi.org/10.1007/s42452-020-2116-6>.
- [3] Li H, Ju Y, Zhang C. Optimization of supercritical carbon dioxide recompression Brayton cycle considering anti-condensation design of centrifugal compressor. *Fuel* 2016;180:694–717. <https://doi.org/10.1016/j.enconman.2022.115207>.
- [4] Crespi F, Rodríguez de Arriba P, Sánchez D, Ayub A, Di Marcoberardino G, Invernizzi CM, Martínez GS, Iora P, Di Bona D, Binotti M, Manzolini G. Thermal efficiency gains enabled by using CO₂ mixtures in supercritical power cycles. *Energy* 2022;238:121899. <https://doi.org/10.1016/j.energy.2021.121899>.
- [5] Olumayegun O, Meihong W, Greg K. Closed-cycle gas turbine for power generation: a state-of-the-art review. *Energy Convers Manag* 2022;254:115207. <https://doi.org/10.1016/j.fuel.2016.04.074>.
- [6] Wright SA, Radel RF, Vernon ME, Rochau GE, Pickard PS. SANDIA REPORT. Operation and Analysis of a Supercritical CO₂ Brayton Cycle 2012.
- [7] Luu MT, Milani D, McNaughton R, Abbas A. Advanced control strategies for dynamic operation of a solar-assisted recompression supercritical CO₂ Brayton power cycle. *Appl Therm Eng* 2018;136:682–700. <https://doi.org/10.1016/j.applthermaleng.2018.03.021>.
- [8] Clementoni EM, Cox TL, King MA, Rahner KD. Transient Power Operation of a Supercritical Carbon Dioxide Brayton Cycle 2017.
- [9] Moissevsev A, Kulesza KP, Sienicki JJ. Control system options and strategies for supercritical CO₂ cycles. <https://doi.org/10.2172/958037>; 2009.
- [10] Heifetz A, Vilim R. Turbine bypass, mass inventory, and mixed-mode generator power control of S-CO₂ recompression cycle. *Nucl Technol* 2015;189:268–77. <https://doi.org/10.13182/NT13-113>.
- [11] Oh BS, Jeong Y, Cho SK, Lee JI. Controllability of S-CO₂ power system coupled small modular reactor with improved compressor design. *Appl Therm Eng* 2021; 192:116957. <https://doi.org/10.1016/j.applthermaleng.2021.116957>.
- [12] Reay DA. Compact heat exchangers: a review of current equipment and R&D in the field. *Heat Recovery Syst CHP* 1994;14:459–74. [https://doi.org/10.1016/0890-4332\(94\)90050-7](https://doi.org/10.1016/0890-4332(94)90050-7).
- [13] Jiang Y, Liese E, Zitney SE, Bhattacharyya D. Design and dynamic modeling of printed circuit heat exchangers for supercritical carbon dioxide Brayton power cycles. *Appl Energy* 2018;231:1019–32. <https://doi.org/10.1016/j.apenergy.2018.09.193>.
- [14] Park JH, Kwon JG, Kim TH, Kim MH, Cha JE, Jo HJ. Experimental study of a straight channel printed circuit heat exchanger on supercritical CO₂ near the critical point with water cooling. *Int J Heat Mass Tran* 2020;150:119364. <https://doi.org/10.1016/j.ijheatmasstransfer.2020.119364>.
- [15] Marchionni M, Bianchi G, Tassou SA. Techno-economic assessment of Joule-Brayton cycle architectures for heat to power conversion from high-grade heat sources using CO₂ in the supercritical state. *Energy* 2018;148:1140–52. <https://doi.org/10.1016/J.ENERGY.2018.02.005>.
- [16] Shiferaw D, Carrero J, Pierres RL. Economic analysis of sCO₂ cycles with PCHE Recuperator design optimisation 2016.
- [17] Fuller R, Preuss J, Noall J. Turbomachinery for supercritical CO₂ power cycles. Proceedings of the ASME Turbo Expo. American Society of Mechanical Engineers Digital Collection 2012;5:961–6. <https://doi.org/10.1115/GT2012-68735>.
- [18] Bianchi G, Saravi SS, Loeb R, Tsamos KM, Marchionni M, Leroux A. Design of a high-temperature heat to power conversion facility for testing supercritical CO₂ equipment and packaged power units. *Energy Proc* 2019;161:421–8. <https://doi.org/10.1016/J.EGYPRO.2019.02.109>.
- [19] T Gamma - Gamma Technologies Inc 2020. GT-SUITE-Flow Theory Manual 2020.
- [20] Gnielinski V. New equation for heat and mass transfer in turbulent pipe and channel flow. *Int Chem Eng* 1976;16:359–68.

- [21] Dittus FW, Boelter LMK. Heat transfer in automobile radiators of the tubular type. *Int Commun Heat Mass Tran* 1985;12:3–22. [https://doi.org/10.1016/0735-1933\(85\)90003-X](https://doi.org/10.1016/0735-1933(85)90003-X).
- [22] Marchionni M, Chai L, Bianchi G, Tassou SA. Numerical modelling and transient analysis of a printed circuit heat exchanger used as recuperator for supercritical CO₂ heat to power conversion systems. *Appl Therm Eng* 2019;161:114190. <https://doi.org/10.1016/j.applthermaleng.2019.114190>.
- [23] Brkić D. Review of explicit approximations to the Colebrook relation for flow friction. *J Petrol Sci Eng* 2011;77:34–48. <https://doi.org/10.1016/J.PETROL.2011.02.006>.
- [24] Prosperetti A. A generalization of the Rayleigh–Plesset equation of bubble dynamics. *Phys Fluids* 1982;25:409. <https://doi.org/10.1063/1.863775>.
- [25] Marchionni M, Bianchi G, Karvountzis-Kontakiotis A, Pesyridis A, Tassou SA. An appraisal of proportional integral control strategies for small scale waste heat to power conversion units based on Organic Rankine Cycles. *Energy* 2018;163:1062–76. <https://doi.org/10.1016/J.ENERGY.2018.08.156>.
- [26] Saravi SS. An investigation into sCO₂ compressor performance prediction in the supercritical region for power systems. *Energy Proc* 2019;161:403–11. <https://doi.org/10.1016/J.EGYPRO.2019.02.098>.
- [27] Marchionni M, Saravi SS, Bianchi G, Tassou SA. Modelling and performance analysis of a supercritical CO₂ system for high temperature industrial heat to power conversion at off-design conditions. 3rd European sCO₂ conference; 2019. <https://doi.org/10.17185/dupublico/48908>.
- [28] Wright SA, Radel RF, Vernon ME, Rochau GE, Pickard PS. Operation and Analysis of a Supercritical CO₂ Brayton Cycle 2010. <https://doi.org/10.2172/984129>.
- [29] Dyreby JJ, Klein SA, Nellis GF, Reindl DT. Modeling Off-Design and Part-Load Performance of Supercritical Carbon Dioxide Power Cycles 2013.
- [30] Samson. Type 3252 high-pressure valve. (online). <https://www.samsoncontrols.net/heavydutyindustrialapplication2.html>.
- [31] Lemmon EW, Huber ML, McLinden MO. NIST standard reference database 23: reference fluid thermodynamic and transport properties-REFPROP, version 9.1, natl std. Ref. Data series (NIST NSRDS), national institute of standards and technology, gaithersburg, MD (online), https://tsapps.nist.gov/publication/get_pdf.cfm?pub_id=912382; 2007.
- [32] Lennartson B, Kristiansson B. Evaluation and tuning of robust PID controllers. *IET Control Theory & Appl* 2009;3:294–302. <https://doi.org/10.1049/iet-cta:20060450>.